CORROSION SCIENCE AND TECHNOLOGY, Vol.23, No.1(2024), pp.41~53
[Research Paper]
pISSN 1598-6462 / eISSN 2288-6524
DOI: https://doi.org/10.14773/cst.2024.23.1.41

Nano-engineering of Hybrid Titanium Oxide Structure (TiO_2) using Pore-widening Concentration for Enhanced Superhydrophilicity

Yeji Choi[1,††] and Chanyoung Jeong[1,2,†,††]

[1]*Department of Advanced Materials Engineering, Dong-eui University, Busan, 47340, Korea*
[2]*The Research Institute of Advanced Functional Surface Engineering, Busan, 47340, Korea*
(Received January 05, 2024; Revised January 24, 2024; Accepted January 25, 2024)

Titanium alloy is gaining attention in the medical industry due to its excellent biocompatibility and osteoconductivity. However, the natural oxide film on the titanium surface is insoluble, resulting in inadequate bone adhesion. Therefore, it is necessary to optimize the contact between biological tissues and implant surfaces, and alter the chemical composition and morphological characteristics of the implant surface. In this study, the anodization method was applied to titanium surface treatment to form a uniform and robust oxide film. Subsequently, a chemical process, pore-widening, was employed to change the morphological characteristics of the oxide film. The concentration of the pore-widening solution was varied at 2, 4, 6, and 8 wt% and the process time was set at 30 and 60 minutes. As the concentration of the pore-widening solution increased the pore diameter of the oxide film increased. Notably, at 6 wt% for 60 minutes, the oxide film exhibited a coexistence of pillars and pores. Based on this, it was determined that surface roughness increased with higher concentration and longer process time. Additionally, the presence of pillars and pores structures maximized hydrophilicity. This study provides insights into enhancing the surface properties of titanium for improved performance in medical implants.

Keywords: *Anodization, Pore-widening concentration, Titanium, Hybrid titanium oxide nanostructure, Superhydrophilicity*

1. Introduction

Titanium (Ti) is a lightweight metal widely utilized in various industries such as construction, shipbuilding, and automotive due to its excellent mechanical properties and heat resistance [1-4]. Particularly noteworthy in the medical industry, titanium stands out as an implant material in dentistry and orthopedic surgery, owing to its superior biocompatibility [1-4]. Titanium exhibits an affinity to oxygen when exposed to air, forming a thermodynamically and chemically stable natural oxide film on its surface. This phenomenon inhibits surface corrosion reactions, ensuring long-term corrosion resistance and durability [5-8].

However, the natural oxide film on titanium is insoluble, leading to a weak bond with bone and prolonging the healing period when used as an implant material [9-12]. To address this issue, physical methods such as oxidation treatment and etching have been employed for surface modification. Nevertheless, these processes can result in the formation of impurity particles on the material surface, compromising reproducibility and potentially causing issues within the human body due to the generation of harmful substances [13-16]. Therefore, to enhance osseointegration and optimize the contact state between biological tissues and implant surfaces, it is essential to modify the chemical composition and morphological characteristics of the implant surface for improved bone conductivity [17-19]. Various surface treatment methods, including plasma electrolytic oxidation, coating, and anodization processes, exist as electrochemical surface treatments [20-22]. Among them, the anodization process is a prominent surface treatment technology that forms a uniform and dense nano- and micro-scale oxide film on metal surfaces through electrochemical methods [23]. The porous structure of the oxide film formed by anodization not only increases the contact area with bone during implantation but also serves as a means to deliver growth

†Corresponding author: cjeong@deu.ac.kr
††These authors contributed equally to this work as the first author.
Yeji Choi: Graduate Student, Chanyoung Jeong: Professor

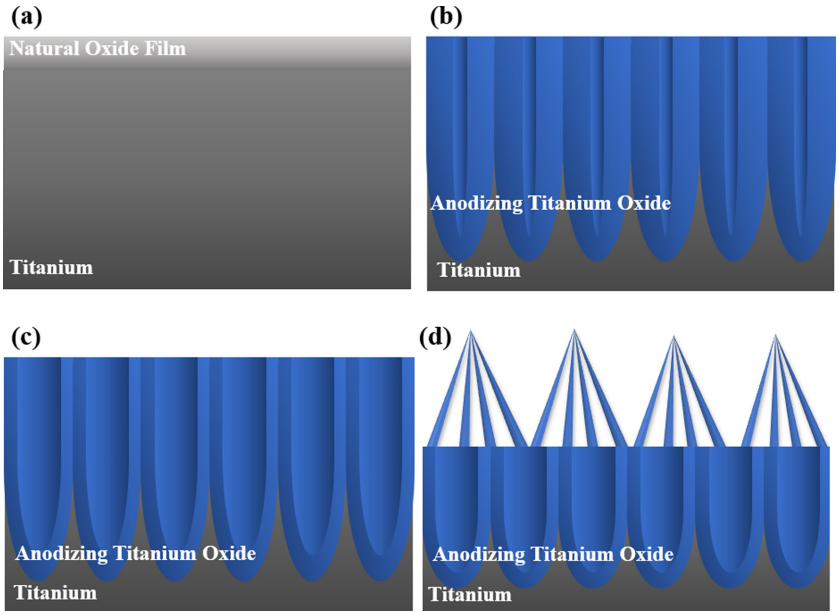

Fig. 1. (a) Untreated Titanium, (b) the morphology of the oxide film after anodization, (c) the morphology of the oxide film with expanded pores through Pore-widening process, (d) the pillar-on-pore structure formed through Pore-widening process

factors associated with bone regeneration [24-26]. Recently, there has been growing interest in porous nanostructures, leading to active research on structures such as micro-multilayers. Anodization processes suitable for forming porous structures are gaining attention due to their advantages, including ease of fabrication and uniformity of pore patterns [27-29].

Currently, the anodization process allows for the variation of the thickness of the oxide film based on various experimental variables such as electrolyte composition, type, applied time, and voltage [30-32]. However, the formation of functional surfaces with three-dimensional pore structures has proven somewhat challenging, as the process typically results in two-dimensional pore structures [33]. Nevertheless, by incorporating a pore-widening (PW) process after anodization, it becomes possible to precisely control the oxide film and create sharp pillar structures. This refinement enables the fabrication of more effective functional surfaces [34-36].

In this context, there exists a difference between the pore structure formed by anodization and the pillar structure formed through the PW process. The pore structure formed by anodization is characterized by a continuous pattern on the surface in contact with the liquid, whereas the pillar structure formed by the PW process exhibits a discontinuous pattern [37]. When both pore and pillar structures coexist, applying a liquid to the surface results in the implementation of a hydrophilic surface [38,39]. Fig. 1 illustrates schematic representations of the oxide film morphology for each process. Panel (a) shows the untreated Titanium, Panel (b) represents the pore structure formed by anodization, while panel (c) shows the oxide film where the pore size has increased through the PW process following anodization. Panel (d) represents an oxide film where the PW process has been applied to partially dissolve the continuous pore structure, resulting in the coexistence of sharp pillar and pore structures. This configuration maximizes the non-surface area, enabling the realization of high wettability. Wettability, the formation of a composite interface among gas, liquid, and solid phases, is primarily confirmed through the numerical value of the contact angle [40]. When the contact angle between the interface and the liquid is below 30°, it is termed hydrophilic, and below 10° is referred to as superhydrophilic [41-42]. Therefore, a systematic process based on the anodization method should be employed to form the oxide film, enabling the creation of surfaces with various functions, such as cell adhesion, in the medical industry [43].

This study conducted experiments on Ti-Grade 4 material by considering the concentration and duration of

the pore-widening (PW) process solution as variables after the anodization process. The goal was to investigate the morphology and composition of the formed oxide film and observe differences in surface roughness and wettability.

2. Experimental Methods

In this study, Ti-Grade 4 sheets with dimensions of 25 × 30 × 1 mm were utilized as the working area. To remove surface impurities, the sheets underwent ultrasonic cleaning for 10 minutes each in acetone, ethanol, and distilled water, sequentially, followed by drying. A mixture of perchloric acid ($HClO_4$) and acetic acid (CH_3COOH) in a 1:5 ratio was stabilized at room temperature. Titanium and platinum electrodes were fixed to the working and counter electrodes, respectively. Electrolytic polishing was then carried out for 10 minutes at 35 V to remove the natural oxide film. Subsequently, an anodization process was conducted using a DC power supply with a voltage of 40 V for 6 hours in an electrolyte composed of 1 M distilled water (H_2O) and 0.07 M ammonium fluoride (NH_4F) in ethylene glycol ($C_2H_6O_2$). Fig. 2 illustrates the schematic diagram of anodization and PW Process. To maintain a temperature of 0 ºC, a dual-jacketed beaker and a water-cooled chiller were employed to circulate cooling water. Subsequently, to increase the non-surface area of the pores in the anodization film, PW process was conducted by immersing the samples in 2, 4, 6, 8 wt% chromic acid (H_2CrO_4) at 65 ºC for 30 and 60 minutes. After completing all processes, the samples were washed in sequence with acetone, ethanol, and distilled water. For the observation of the thickness and morphology of the oxide film formed on the surface after the PW process, Field Emission-Scanning Electron Microscopy (FE-SEM, Jeol, JSM-IT800) was utilized at 65 ºC for 30 and 60 minutes. The chemical composition of the oxide film was qualitatively and quantitatively analyzed using Energy Dispersive Spectroscopy (EDS). Subsequently, the roughness of the oxide film according to the concentration and time of the PW solution was observed using Atomic Force Microscopy (AFM, NITECH, SPA-400). To observe wettability based on surface roughness, a Contact Angle Meter (CAM, Smart drop standard) was used. The contact angle was measured by placing 3 μL of distilled water on each sample, measuring the contact angle five times, and calculating the average value.

3. Results

This study aimed to observe the differences in the morphology and thickness of the oxide film resulting from changes in the concentration and treatment time of the PW process solution after anodization of Ti-Grade 4 sheets. Additionally, the surface roughness and wettability characteristics based on the morphology of the oxide film produced under each condition were investigated. The

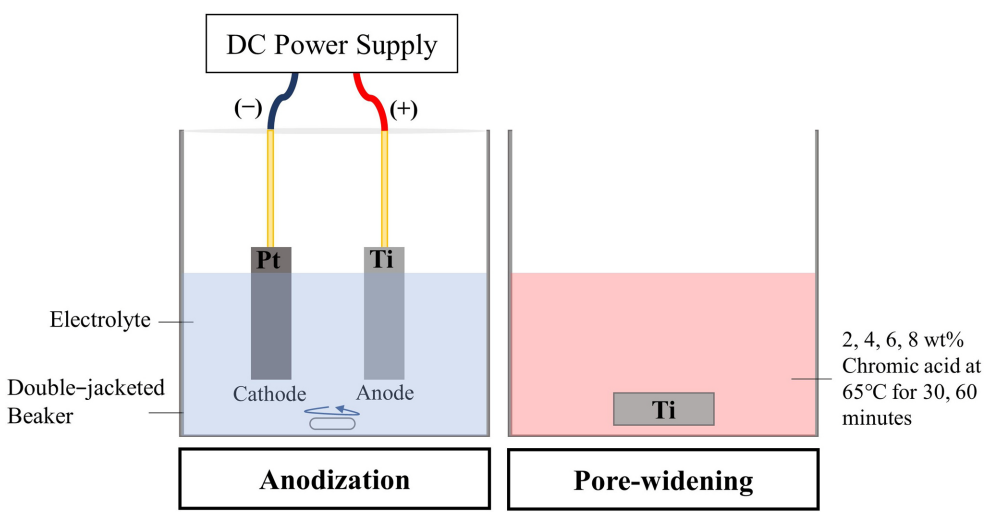

Fig. 2. Schematic representation of the experimental method

chemical composition of untreated titanium used in the study was analyzed through Energy Dispersive Spectroscopy (EDS), and the results are presented in Table 1.

Fig. 3 presents FE-SEM images observing the oxide film formed on titanium through 6 hours of anodization. The corresponding pore diameter, pore spacing, thickness, and solid fraction are specified in Table 2. The images in Fig. 3 confirm the formation of a porous oxide film through 6 hours of anodization. The pore size measures 65.03 ± 8.21 nm, pore spacing is 75.06 ± 8.28 nm, oxide film thickness is 5.93 ± 0.37 μm, and the solid fraction is measured at 0.53. The solid fraction (f_{SL}) was calculated using equation (1), where a represents the pore spacing, and r represents the radius of the pores [29].

$$f_{SL} = 1 - \frac{2\pi r^2}{\sqrt{3}a^2} \quad (1)$$

The qualitative and quantitative analysis of the components in the oxide film formed through anodization

Table 1. Chemical composition of untreated Ti

Element	Wt (%)
Ti	92.95
O	4.11
C	2.94

Table 3. Chemical composition analysis of oxide film after 6 hours of anodization using EDS

Anodization 6hrs.	
Element	Wt%
Titanium (Ti)	50.70
Oxygen (O)	45.83
Fluorine (F)	3.47

is presented in Table 3. When compared to the untreated sample, the oxygen (O) content increased from 4.11 wt% to 45.83 wt%, while the titanium (Ti) content decreased from 92.95 wt% to 50.70 wt%. This suggests that during anodization, cations generated from the titanium substrate and oxygen emitted from the cathode react to form the oxide film, leading to an increase in oxygen content and a decrease in titanium content. The presence of fluorine (F) is attributed to the influence of NH_4F in the anodization electrolyte.

Fig. 4 illustrates the morphology of the oxide film after 30 minutes of the PW process at different solution concentrations. It is evident from the top view that a porous oxide film has formed, and as the solution concentration increases, the pore diameter also increases. At 8 wt%, the expansion of the pores results in thinning of the pore walls, indicating dissolution of the oxide film. Based on Fig. 4, the pore diameter, pore spacing,

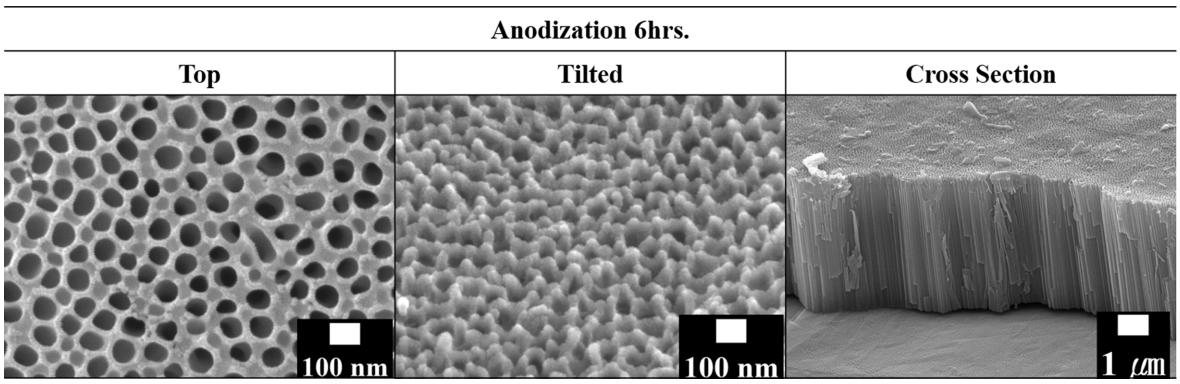

Fig. 3. Morphology of the oxide film formed after 6hours of anodization

Table 2. Measured pore diameter (D_p), interpore distance (D_{int}), oxide film thickness and Solid Fraction (f_{SL}) after 6 hours of anodization

Anodization 6hrs.			
D_p (nm)	D_{int} (nm)	Thickness (μm)	Solid Fraction
65.03 ± 8.21	75.06 ± 8.28	5.93 ± 0.37	0.53

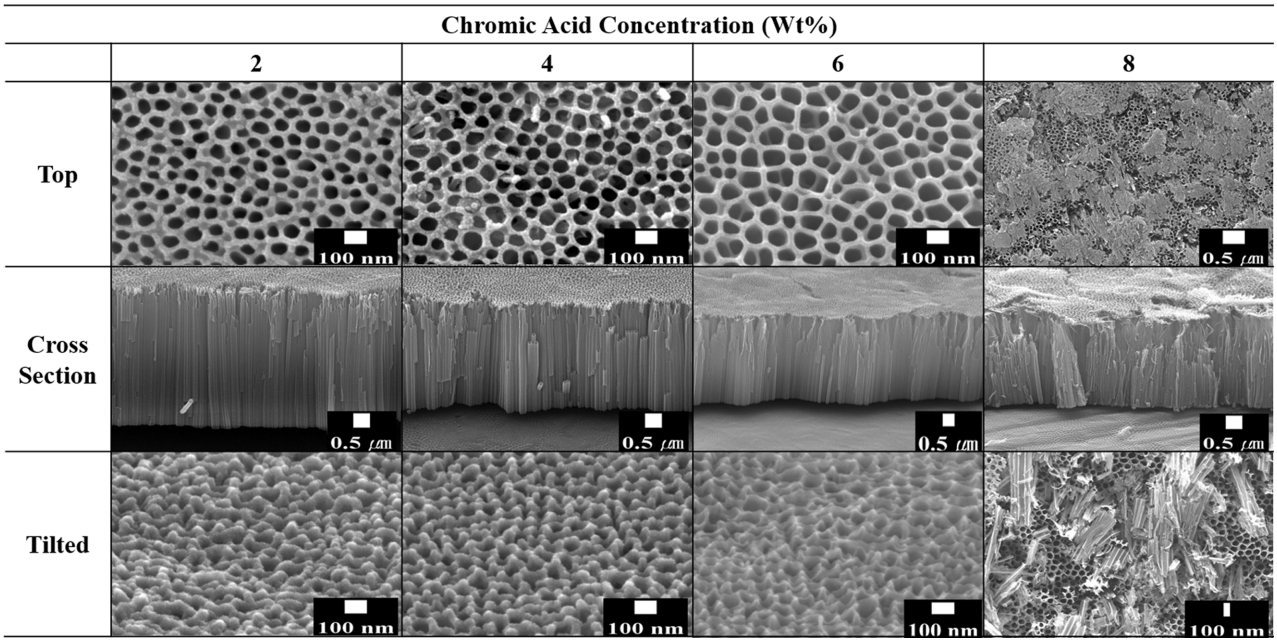

Fig. 4. Morphology results of oxide film after 30 minutes of Pore-widening process as observed through FE-SEM analysis

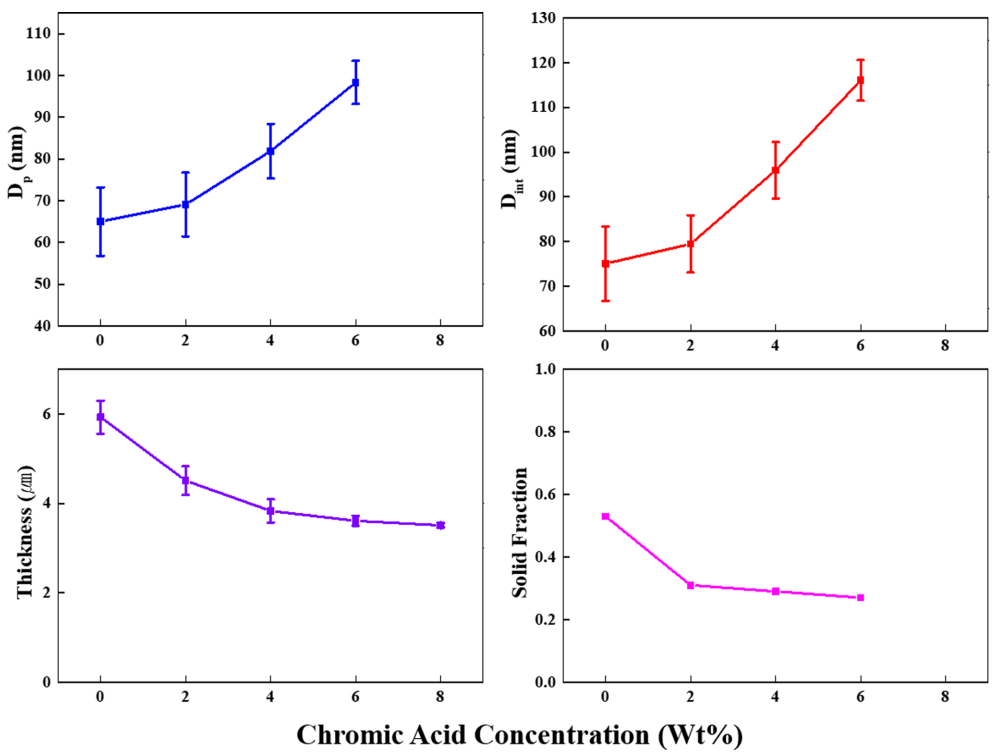

Fig. 5. Graphs illustrating the measured pore diameter (D_p), interpore distance (D_{int}), thickness and Solid Fraction (f_{SL}) of the oxide film after 30 minutes Pore-widening process

thickness, and solid fraction of the oxide film were measured, and the results are presented in the graph in Fig. 5 and Table 4. As the PW solution concentration increases from 2 wt% to 6 wt%, the pore diameter increases from 69.09 ± 7.64 nm to 98.35 ± 5.17 nm, and the pore spacing increases from 79.46 ± 6.42 nm to 116.04

Table 4. Measured pore diameter (D_p), interpore distance (D_{int}), thickness and Solid Fraction (f_{SL}) of the oxide film after 30 minutes Pore-widening process

	Chromic Acid Concentration (Wt%)			
	2	4	6	8
D_p (nm)	69.09 ± 7.64	81.87 ± 6.57	98.35 ± 5.17	N/A
D_{int} (nm)	79.46 ± 6.42	95.98 ± 6.29	116.04 ± 4.56	N/A
Thickness (μm)	4.51 ± 0.32	3.83 ± 0.26	3.61 ± 0.11	3.51 ± 0.05
Solid Fraction	0.31	0.29	0.27	N/A

± 4.56 nm. However, at 8 wt%, these measurements were not obtained. The thickness of the oxide film decreases from 4.51 ± 0.32 μm at 2 wt% to 3.51 ± 0.05 μm at 8 wt%. Fig. 5 indicates that as the concentration of the PW solution increases, the graphs of pore diameter and pore spacing steeply rise. This suggests that the chemical reaction between the solution and the oxide film becomes more active, leading to an increased etching rate. Consequently, the enlargement of pore diameter, reduction of pore wall thickness, and decrease in the thickness of the oxide film occur more rapidly.

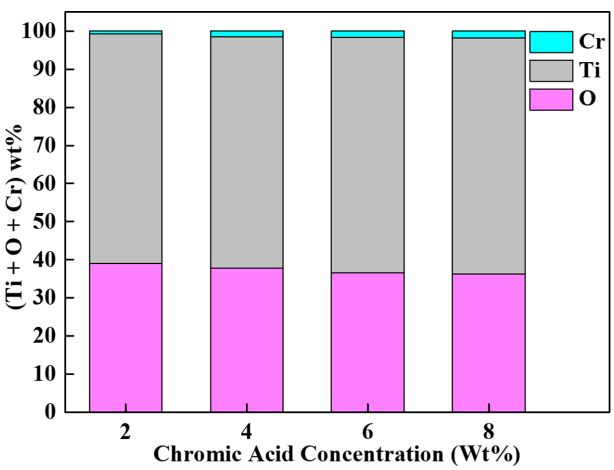

Fig. 6. Sum of titanium (Ti), oxygen (O) and chrome (Cr) content observed through EDS following 30 minutes Pore-widening process

After 30 minutes of the PW process, the qualitative and quantitative analysis of the oxide film was performed, and the composition of each component is presented in Table 5. The sum of detected elements is shown in Fig. 6. For the 2 wt% concentration of the PW solution, the oxygen content was found to be 39.07 wt%, and the titanium content was 60.13 wt%. In the case of 8 wt%, the oxygen content was 36.32 wt%, and the titanium content was 61.85 wt%. This indicates that as the concentration of the PW solution increases, the expansion of pores progresses, leading to a decrease in the thickness of the oxide film. Consequently, the oxygen content decreases, and the titanium content increases. The detected chromium (Cr) is presumed to result from the PW process solution, chromic acid.

Fig. 7 illustrates the morphology of the oxide film after 60 minutes of the PW process at different solution concentrations. The Top View images show that as the concentration increases, the pore diameter increases while the thickness of the pore walls decreases. At a concentration of 6 wt%, the oxide film exhibits a combination of pillar and pore structures. However, at 8 wt%, the increase in pore diameter leads to a decrease in the thickness of the pore walls, resulting in the collapse of the pillar and pore structures and an entangled appearance. Quantitative measurements are presented in Table 6 and graphically represented in Fig. 8. As the

Table 5. Composition of oxide film after 30 minutes of pore-widening process analyzed by EDS

	Chromic Acid Concentration (Wt%)			
Element (wt%)	2	4	6	8
O	39.07	37.84	36.65	36.32
Ti	60.13	60.71	61.71	61.85
Cr	0.80	1.45	1.64	1.83

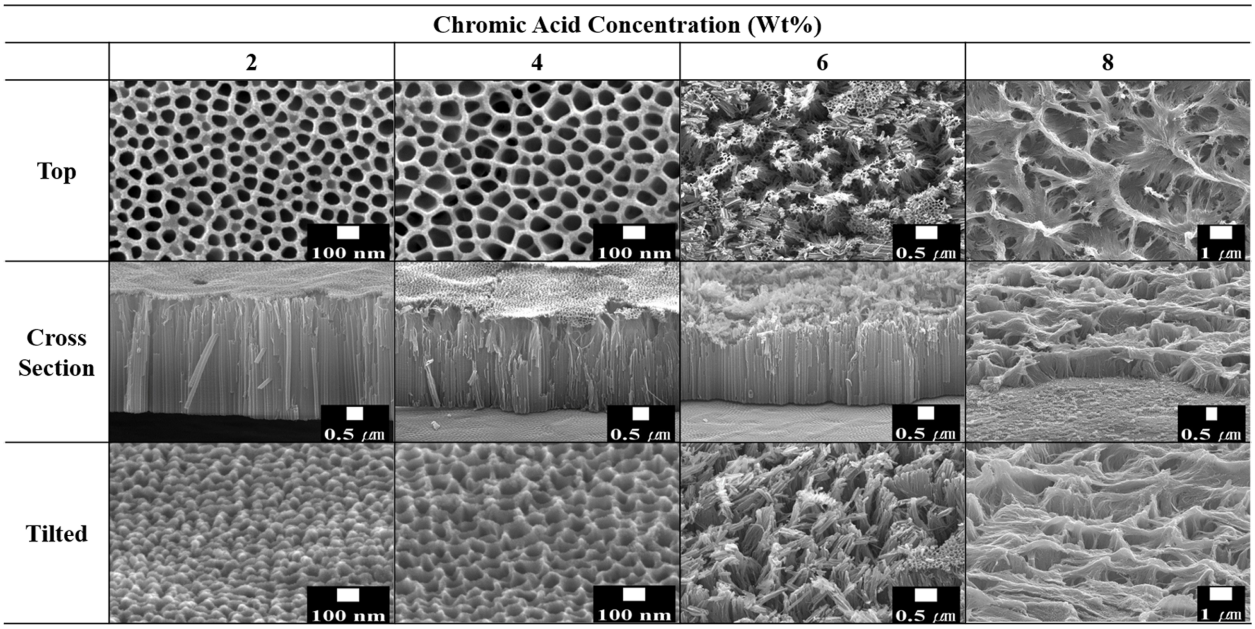

Fig. 7. Morphology results of oxide film after 60 minutes of Pore-widening process as observed through FE-SEM analysis

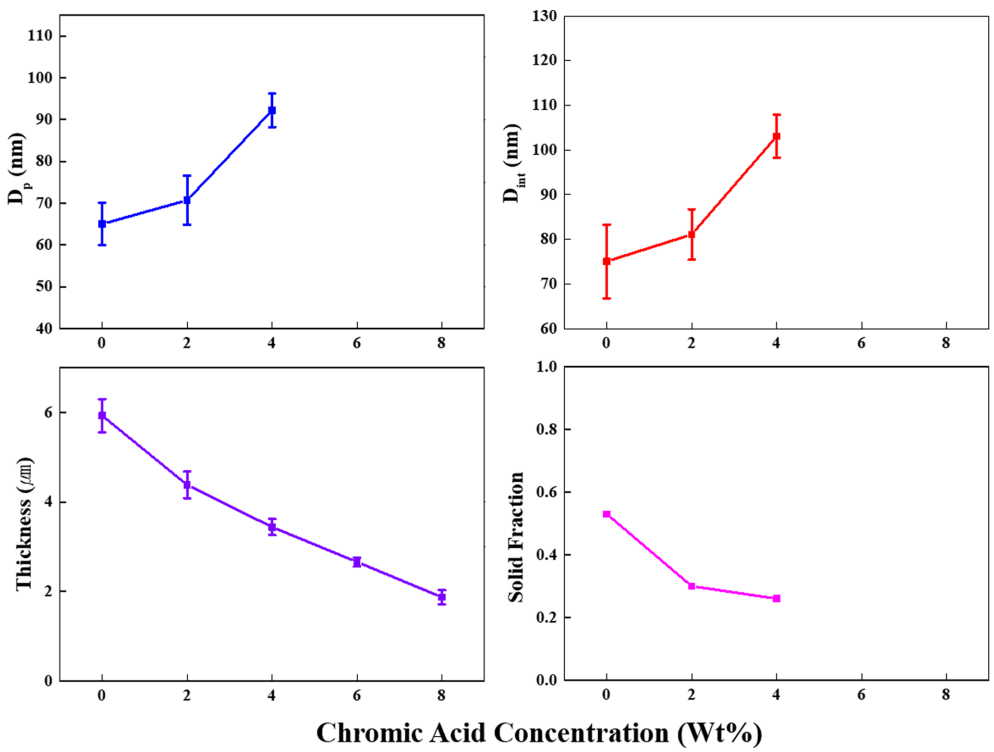

Fig. 8. Graphs illustrating the measured pore diameter (D_p), interpore distance (D_{int}), thickness and Solid Fraction (f_{SL}) of the oxide film after 60 minutes Pore-widening process

concentration of the PW solution increases from 2 wt% to 4 wt%, the pore diameter increases from 70.71 ± 5.88 nm to 92.24 ± 4.01 nm, and the pore spacing increases from 81.09 ± 5.66 nm to 103.08 ± 4.76 nm, with a decrease in standard deviation. However, the thickness of the oxide film decreases from 4.38 ± 0.30 μm to 1.87 ± 0.04 μm, and the solid fraction decreases from 0.30 to 0.26. Measurements for pore diameter, pore spacing, and solid

Table 6. Composition of oxide film after 60 minutes of Pore-widening process analyzed by EDS

	Chromic Acid Concentration (Wt%)			
	2	4	6	8
D_p (nm)	70.71 ± 5.88	92.24 ± 4.01	N/A	N/A
D_{int} (nm)	81.09 ± 5.66	103.08 ± 4.76	N/A	N/A
Thickness (μm)	4.38 ± 0.30	3.44 ± 0.18	2.66 ± 0.10	1.87 ± 0.04
Solid Fraction	0.30	0.26	N/A	N/A

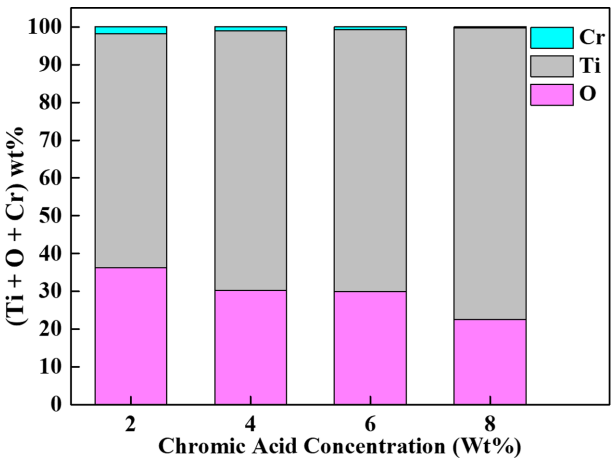

Fig. 9. Sum of titanium (Ti), oxygen (O) and chrome (Cr) content observed through EDS following 60 minutes Pore-widening process

fraction were not obtained at 6 and 8 wt%, indicating that the increased concentration of the chromic acid solution, with its acidic nature, accelerated the etching rate in the strongly acidic environment, leading to rapid dissolution of the oxide film.

Table 7 presents the surface composition analysis results for the oxide film after 60 minutes of the PW process, and the sum of the detected elements is shown in Fig. 9. As the concentration of the PW solution increases, the oxygen content decreases from 36.21 wt% to 22.57 wt%, while the titanium content increases from 61.90 wt% to 77.08 wt%. This suggests that the dissolution rate of the oxide film increases due to the stronger acidic environment with the higher concentration of the PW solution. Comparing the oxygen and titanium content detected after 30 minutes of the PW process (Table 5) to that after 60 minutes, it is evident that the oxygen content decreases, and the titanium content increases with the longer PW process time. This difference indicates that as the PW process time increases, the extent of dissolution of the oxide film intensifies, leading to variations in the oxygen and titanium content.

Fig. 10 provides images for comparing the surface morphology of the oxide film based on the variables of PW process time and concentration. At 2 wt% and 4 wt%, pore structures are observed after both 30 and 60 minutes of the PW process. For 6 wt% at 30 minutes, a pore structure is observed, while at 60 minutes, a morphology change is observed with the coexistence of pillar and pore structures. Additionally, at 8 wt% and 30 minutes, Pillar structures are forming as the oxide film dissolves, and at 60 minutes, the oxide film dissolves rapidly, resulting in a collapsed morphology. In both 30 and 60 minutes of the PW process, higher concentration solutions exhibit faster dissolution reactions, exerting a more significant impact on the etching of the structural elements.

Fig. 11 shows AFM results, including the surface roughness of the final oxide film measured to compare the variables of PW solution concentration and process time. The roughness factor, represented by the Ra value,

Table 7. EDS analysis results, chemical composition after 60 minutes of Pore-widening

	Chromic Acid Concentration (Wt%)			
Element (wt%)	2	4	6	8
O	36.21	30.20	29.87	22.57
Ti	61.90	68.80	69.32	77.08
Cr	1.89	1.00	0.81	0.35

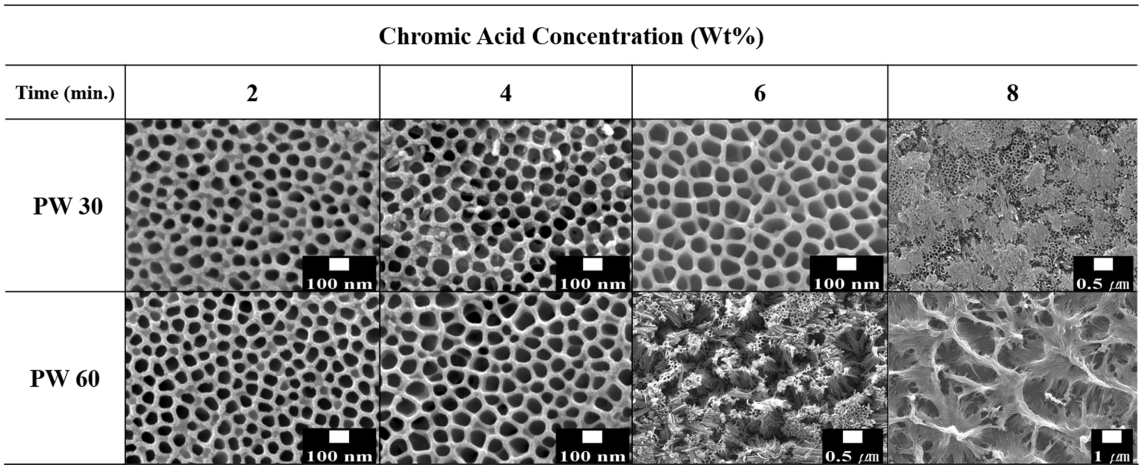

Fig. 10. Morphology of oxide film formed according to Pore-widening times

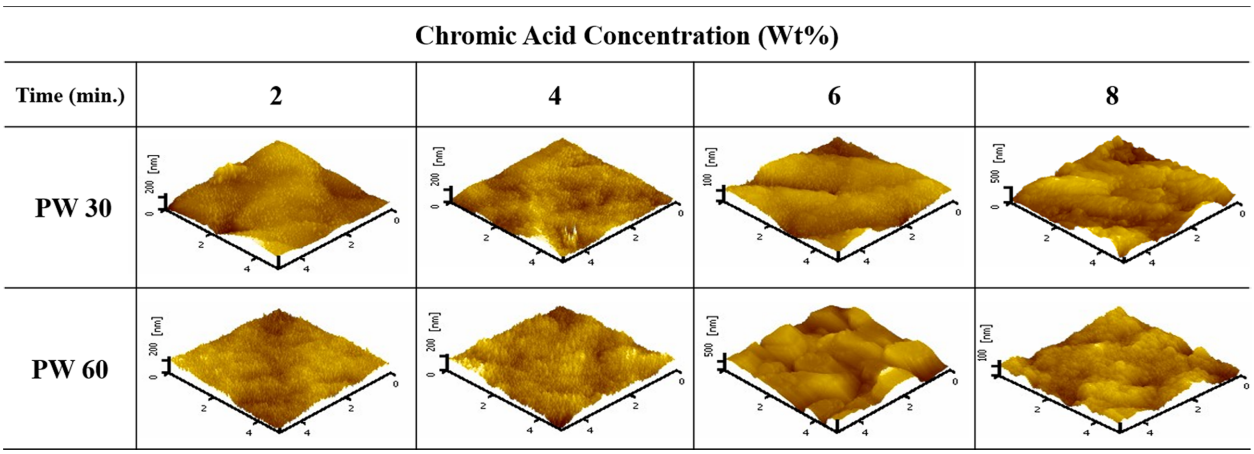

Fig. 11. Surface roughness image of the oxide film according to Pore-widening time and solution concentration

is listed in Table 8. From Fig. 12, it is evident that as the PW process time and solution concentration increase, the surface of the oxide film becomes rougher. This roughening is attributed to the expansion of pore diameters in the oxide film due to the PW process, resulting in thinner pore walls and deeper pore cavities. However, an interesting observation is the decrease in roughness at 8 wt% for 60 minutes in the PW process. This decrease is attributed to the more extensive dissolution of the oxide film in the presence of pillar and pore structures, resulting in a collapsed morphology and reduced roughness.

Fig. 13 presents the contact angles of the oxide film measured to analyze the relationship between surface roughness and wettability concerning the variables of PW solution concentration and process time. The numerical values are listed in Table 9. In the case of the PW 30-minute process, as the PW solution concentration

Table 8. R_a value of the oxide film according to Pore-widening time and solution concentration

Chromic Acid Concentration (Wt%)					
Time (min.)		2	4	6	8
R_a (nm)	PW 30	19.4	21.4	34.92	85.97
	PW 60	20.4	28.11	132.58	90.67

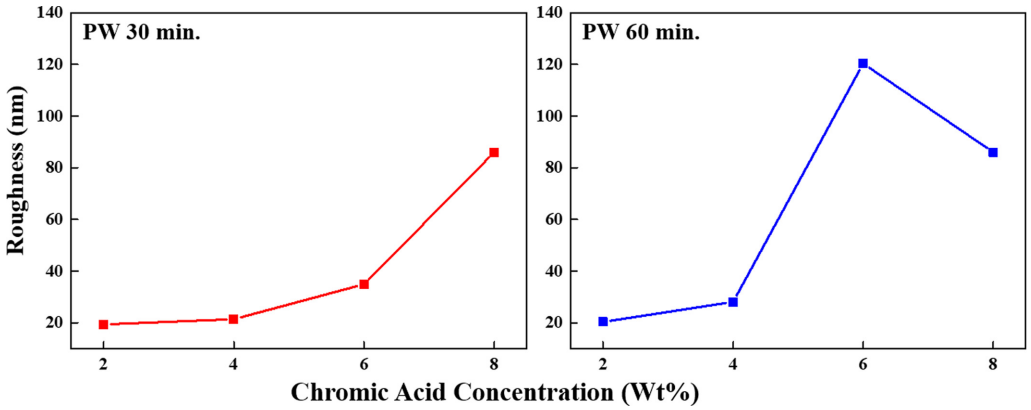

Fig. 12. Changes in R_a value of the oxide film according to Pore-widening time and solution concentration

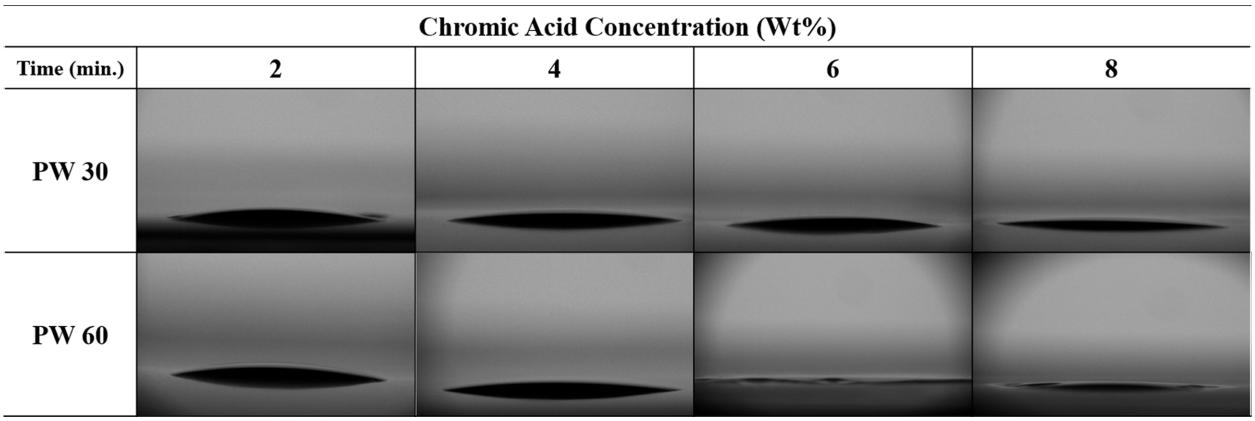

Fig. 13. Comparison of wettability oxide film formed according to Pore-widening time and solution concentration

Table 9. Wettability values of oxide film formed according to Pore-widening time and solution concentration

Chromic Acid Concentration (Wt%)					
Time (min.)		2	4	6	8
Contact Angle (°)	PW 30	16.3 ± 2.35	12.4 ± 1.09	9.81 ± 1.29	4.31 ± 3.10
	PW 60	15.8 ± 3.10	10.1 ± 0.18	0	0

increased, the contact angle decreased from 16.3° to 4.31°, indicating a hydrophilic surface for all samples. In the PW 60-minute process, the contact angle decreased from 15.8° to 10.1°, but measurements were not taken for 6 and 8 wt%. This decrease is attributed to the enlargement of pore diameters and increased surface roughness with higher PW concentrations, leading to a broader surface area in contact with the liquid and an increase in wettability. Additionally, at 6 wt%, the effect of Pillar and pore structures resulted in a superhydrophilic surface, while at 8 wt%, the increased contact area due to the collapsed morphology of the oxide film enhanced wettability.

4. Discussion

This study investigated the morphology and chemical composition of the oxide film formed on Ti-Grade 4 material, with the concentration and processing time of the pore-widening (PW) solution as variables after anodization. The surface roughness and hydrophilic properties resulting from these variations were also examined. After 30 minutes of the PW process, a porous oxide film was observed at concentrations of 2, 4, and 6 wt%, while at 8 wt%, the formation of both pillar and pore structures was observed. Moreover, after 60 minutes

of the PW process, an increase in the pore diameter was observed at concentrations of 2 and 4 wt% compared to the 30-minute process. At 6 wt%, a coexistence of pillar and pore structures was observed. However, at 8 wt%, a more rapid dissolution of the oxide film led to the collapse of the structure beyond the pillar and pore formation, resulting in an entangled structure. This observation suggests that the expansion of pores occurs due to the chromic acid solution, and as the concentration of the PW solution increases, the chemical reaction between the solution and the oxide film becomes more active, accelerating the etching rate.

When comparing the surface roughness of the final oxide film based on the variables of PW solution concentration and processing time, it was observed that, at the same PW processing time, the surface roughness of the oxide film increased with higher concentrations, except for the case of 8 wt% for 60 minutes, where the surface roughness decreased. This trend aligns with the observations made through FE-SEM of the oxide film morphology. Measuring the contact angle based on surface roughness revealed that as the PW processing time and concentration increased, the wettability increased. Notably, at 6 and 8 wt% for 60 minutes, a superhydrophilic surface was achieved. At 6 wt%, the effects of pillar and pore structures were maximized, while at 8 wt%, the entangled structure of the oxide film led to an increase in contact area with the liquid, increasing hydrophilicity.

The coexistence of pillar and pore structures resulting in a superhydrophilic titanium surface can find applications in the medical industry, such as cell adhesion. To further advance the utilization of these structures in various industrial fields related to surface phenomena, it is essential to systematically establish pore-widening processes tailored to different materials. Therefore, additional research is needed for the systematic application and commercialization of these surface structures in various industries.

References

1. N. K. Kuromoto, R. A. Simao, and G. A. Soares, Titanium Oxide Films Produced on Commercially Pure Titanium by Anodic Oxidation with Different Voltage, *Materials Characterization*, **58**, 114 (2007). Doi: https://doi.org/10.1016/j.matchar.2006.03.020
2. W. J. Lee, M. Alhoshan, W. H. Smyrl, Titanium Dioxide Nanotube Arrays Fabricated by Anodizing Process: Electrochemical Properties, *Journal of The Electrochemical Society,* **153**, B499 (2006). Doi: https://doi.org/10.1149/1.2347098
3. H. Li, J. Qu, Q. Cui, H. Xu, H. Luo, M. Chi and S. Dai, TiO_2 Nanotube Arrays Grown in Ionic Liquids: High-efficiency in Photocatalysis and Pore-widening, *Journal of Materials Chemistry,* **21**, 9487 (2007). Doi: https://doi.org/10.1039/c1jm11540e
4. Y. Park and C. Jeong, Surface Modification of Functional Titanium Oxide to Improve Corrosion Resistance, *Corrosion Science and Technology,* **20**, 256 (2021). Doi: https://doi.org/10.14773/cst.2021.20.5.256
5. S. Yoriya and C. A. Grimes, Self-Assembled TiO2 Nanotube Arrays by Anodization of Titanium in Diethylene Glycol: Approach to Extended Pore Widening, *Langmuir*, **26**, 417 (2010). Doi: https://doi.org/10.1021/la9020146
6. E. Byon, S. Moon, S. B. Cho, C. Jeong, Y. Jeong and Y. T. Sul, Electrochemical Property and Apatite Formation of Metal ion Implanted Titanium for Medical Implants, *Surface and Coatings Technology,* **200**, 1018 (2005). Doi: https://doi.org/10.1016/j.surfcoat.2005.02.133
7. S. Moon, C. Jeong, E. Byon and Y. Jeong, Electrochemical Behavior of titanium in NaOH Solutions, *ECS Transactions,* **1**, 151 (2006). Doi: https://doi.org/10.1149/1.2215498
8. S. Berger, J. Kunze, P. Schmuki, D. Leclere, A. T. Valota, P. Skeldon and G. E. Thompson, A lithographic Approach to Determine Volume Expansion Factors during Anodization: Using the Example of Initiation and Growth of TiO2-Nanotubes, *Electrochimica Acta*, **54**, 5942 (2009). Doi: https://doi.org/10.1016/j.electacta.2009.05.064
9. P. Li, S. Dai, D. Dai, Z. Zou, R. Wang, P. Zhu and F. Huang, Influence of the Microstructure of Sputtered Ti Films on the Anodization toward TiO2 Nanotubes Arrays, *Chemical Physics Letters*, **826**, 140675 (2023). Doi: https://doi.org/10.1016/j.cplett.2023.140675
10. J. H. Xing, Z. B. Xia, J. F. Hu, Y. H. Zhang and L. Zhong, Growth and Crystallization of Titanium Oxide Films at Different Anodization Modes, *Journal of The Electrochemical Society*, **160**, C239 (2013). Doi: https://doi.org/10.1149/2.070306jes
11. X. Yu, Y. Li, W. Ge, Q. Yang, N. Zhu and K. Kalantarzadeh, Formation of Nanoporous Titanium Oxide Films on Silicon Substrates Using and Anodization Process,

Nanotechnology, **17**, 808 (2006). Doi: https://doi.org/10.1088/0957-4484/17/3/033

12. S. H. Kim and C. Jeong, Feasibility of Machine Learning Algorithms for Predicting the Deformation of Anodic Titanium Films by Modulating Anodization Processes, *Materials*, **14**, 1089 (2021). Doi: https://doi.org/10.3390/ma14051089
13. J. M. Jáquez-Muñoz, C. Gaona-Tiburcio, C. T. Méndez-Ramírez, M. Á. Baltazar-Zamora, F. Estupinán-López, R. G. Bautista-Margulis, and F Almeraya-Calderón, Corrosion of Titanium Alloys Anodized Using Electrochemical Techniques, *Metals,* **13**, 476 (2023). Doi: https://doi.org/10.3390/met13030476
14. A. K. Sharma, Anodizing Titanium for Space Applications, *Thin Solid Films*, **208**, 48 (1992). Doi: https://doi.org/10.1016/0040-6090(92)90946-9
15. M. Izmir and B. Ercan, Anodization of Titanium Alloys for Orthopedic Applications, *Frontiers of Chemical Science and Engineering*, **13**, 28 (2019). Doi: https://doi.org/10.1007/s11705-018-1759-y
16. C. C. Chen, J. H. Chen and C. G. Chao, Post-treatment Method of Producing Ordered Arrays of Anodic Aluminum Oxide Using General Purity Commercial (99.7%) Aluminum, *Japanese Journal of Applied Physices*, **44**, 1529 (2005). Doi: https://doi.org/10.1143/JJAP.44.1529
17. C. Jeong, J. Lee, K. Sheppard and C. H. Choi, Air-impregnated Nanoporous Anodic Aluminum Oxide Layers for Enhancing the Corrosion Resistance of Aluminum, *Langmuir*, **31**, 11040 (2015). Doi: https://doi.org/10.1021/acs.langmuir.5b02392
18. H. Wang, Z. Huang, L. Zhang, J. Ding, Z. Ma, Y. Liu and H. Yang, Engineering of Highly Ordered TiO2 Nanopore Arrays by Anodization, *Applied Surface Science*, **377**, 335 (2016). Doi: https://doi.org/10.1016/j.apsusc.2016.03.184
19. C. Yao and T. J. Webster, Anodization: A Promising Nano-Modification Technique Implants for Orthopedic Applications, *Journal of Nanoscience and Nanotechnology*, **6**, 2682 (2006). Doi: https://doi.org/10.1166/jnn.2006.447
20. D. H. Shin and S. J. Kim, Effects of Hard Anodizing and Plasma Ion-Nitriding on Al Alloy for Hydrogen Embrittlement Portection, *Corrosion Science and Technology*, **22**, 221 (2023). Doi: https://doi.org/10.14773/cst.2023.22.4.221
21. F. Keller, M. S. Hunter and D. L. Robinson, Structural Features of Oxide Coatings on Aluminum, *Journal of The Electrochemical Society*, **100**, 411 (1953). Doi: https://doi.org/10.1149/1.2781142
22. J. M. Calderon, P. Drob, C. Vasilescu, S. I. Drob, M. Popa and E. Vasilescu, Oxide Nanolayers Grown on New Ternary Ti Based Alloy Surface by Galvanic Anodizing-Characteristics and Anticorrosion Properties, *Corrosion Science and Technology,* **16**, 257 (2017). Doi: https://doi.org/10.14773/cst.2017.16.5.257
23. H. Masuda, K, Yada and A. Osaka, Self-ordering of Cell Configuration of Anodic Porous Alumina with Large-size Pores in Phosphoric Acid Solution, *Japanese Journal of Applied Physices*, **37**, L1340 (1998). Doi: https://doi.org/10.1143/JJAP.37.L1340
24. Y. Choi and C. Jeong, Influence of Electrolyte on the Shape and Characteristics of TiO_2 during Anodic Oxidation of Titanium, *Corrosion Science and Technology,* **22**, 193 (2023). Doi: https://doi.org/10.14773/cst.2023.22.3.193
25. J. Evertsson, N. A., Vinogradov, G. S. Harlow, F. Carlà, S. R. McKibbin, L. Rullik and E. Lundgren, Self-organization of Porous Anodic Alumina Films Studied in situ by Grazing-incidence Transmission Small-angle X-ray Scattering, *RSC Advances,* **8**, 18980 (2018). Doi: https://doi.org/10.1039/C8RA02913J
26. S. K. Hwang, S. H. Jeong, H. Y. Hwang, O. J. Lee and K. H. Lee, Fabrication of Highly Ordered Pore Array in Anodic Aluminum Oxide, *Korean Journal of Chemical Engineering*, **19**, 467, Doi: https://doi.org/10.1007/BF02697158
27. H. Masuda and K. Fukuda, Ordered Metal Nanohole Arrays Made by a Two-step Replication of Honeycomb Structures of Anodic Alumina, *Science*, **268**, 1466 (1995). Doi: https://doi.org/10.1126/science.268.5216.1466
28. H. Ji and C. Jeong, Fabrication of Superhydrophobic Aluminum Alloy Surface with Hierarchical Pore Nanostructure for Anti-Corrosion, *Corrosion Science and Technology*, **18**, 228 (2019). Doi: https://doi.org/10.14773/cst.2019.18.6.228
29. Y. Park, H. Ji and C. Jeong, Development of Superhydrophilic 6061 Aluminum Alloy by Stepwise Anodization According to Pore-widening Time, *Korean Journal of Metals and Materials,* **58**, 97 (2020). Doi: http://dx.doi.org/10.3365/KJMM.2020.58.2.97
30. A. E. Kozhukhoova, S. P. Du Preez and D. G. Bessarabov, The Effects of Pore Widening and Calcination on Anodized Aluminum Oxide Prepared from Al6082, *Surface and Coatings Technology,* **383**, 125234 (2020). Doi: https://doi.org/10.1016/j.surfcoat.2019.125234
31. H. Ji and C. Jeong, Systematic Control of Anodic Aluminum Oxide Nanostructures for Enhancing the Superhydrophobicity of 5052 Aluminum Alloy, *Materials*, **12**, 3231 (2019). Doi: https://doi.org/10.3390/ma12193231

32. R. Blossey, Self-cleaning Surfaces-Virtual Realities, *Nature Materials,* **2**, 301 (2003). Doi: https://doi.org/10.1038/nmat856
33. C. Jeong, A Study on Functional Hydrophobic Stainless Steel 316L Using Single-Step Anodization and a Self-Assembled Monolayer Coating to Improve Corrosion Resistance, *Coatings,* **12**, 395 (2022). Doi: https://doi.org/10.3390/coatings12030395
34. C. Jeong and C. H. Choi, Single-step Direct Fabrication of Pillar-on-pore hybrid Nanostructures in Anodizing Aluminum for Superior Superhydrophobic Efficiency, *ACS Applied Materials & Interfaces,* **4**, 842 (2012). Doi: https://doi.org/10.1021/am201514n
35. A. B. D. Cassie and S. Baxter, Wettability of Porous Surfaces, *Transactions of the Faraday Society*, **40**, 546 (1944). Doi: https://doi.org/10.1039/TF9444000546
36. M. Tang, J. He, J. Zhou and P. He, Pore-widening with the Assistance of Ultrasonic: A Novel Process for Preparing Porous Anodic Aluminum Oxide Membrane, *Materials Letters,* **60**, 2098 (2006). Doi: https://doi.org/10.1016/j.matlet.2005.12.080
37. J. A. Varela, O. J. Whittemore and E. Longo, Pore Size Evolution during Sintering of Ceramic Oxides,). *Ceramics International,* **16**, 177 (1990). Doi: https://doi.org/10.1016/0272-8842(90)90053-I
38. D. Routkevitch, A.A. Tager, J. Haruyama, D. Almawlawi, M. Moskovits and J. M. Xu, Nonlithographic Nano-wire Arrays: Fabrication, Physics, and Device Applications, *IEEE Trnas. Electron. Devices.,* **43**, 1646 (1996). Doi: https://doi.org/10.1109/16.536810
39. S. Wu, H. Zhou, M. Hao, X. Wei, S. Li, H. Yu and Z. Chen, Fast Response Hydrogen Sensors Based on Anodic Aluminum Oxide with Pore-widening Treatment, *Applied Surface Science,* **380**, 47 (2016). Doi: https://doi.org/10.1016/j.apsusc.2016.02.087
40. Y. H. Ogata, A. Koyama, F. A. Harraz, M. S. Salem and T. Sakka, Electrochemical Formation of Porous Silicon with Medium-sized Pores, *Electrochemistry,* **75**, 270 (2007). Doi: https://doi.org/10.5796/electrochemistry.75.270
41. C. Jeong, J. Jung, K. Sheppard and C. H. Choi, Control of the Nanopore Architecture of Anodic Alumina via Stepwise Anodization with Voltage Modulation and Pore Widening, *Nanomaterials*, **13**, 342 (2023). Doi: https://doi.org/10.3390/nano13020342
42. L. Zaraska, G. D. Sulka and M. Jaskula, Anodic Alumina Membranes with Defined Pore Diameters and Thicknesses Obtained by Adjusting the Anodizing Duration and Pore Opening/Widening Time, *Journal of Solid State Electrochemistry*, **15**, 2427 (2011). Doi: https://doi.org/10.1007/s10008-011-1471-z
43. S. M. Suchitra, P. R. Reddy, and N. K. Udayashankar, Effect of Pore Widening Time on the Structural Aspects of Self-Organized Nanopore Arrays Formed by Anodization of Aluminum in Chromic Acid, *Materialstoday: Proceedings,* **3**, 2042 (2016). Doi: https://doi.org/10.1016/j.matpr.2016.04.107